

## Transmission Performance for WLAN Employing Switched Beamforming Array

Hsueh-Jyh Li, Zong-Hua You, Ta-Chien Yeh  
Graduate Institute of Communication Engineering, National Taiwan University,  
Taipei, Taiwan, R.O.C., email: [hjli@ew.ee.ntu.edu.tw](mailto:hjli@ew.ee.ntu.edu.tw)

### Abstract

In this paper we proposed a vector wideband channel model and use this channel model to compare the transmission performance of the WLAN system using omni-directional antennas and switched beamforming arrays for different channel situations. We found that the greater the difference between the amplitude of the direct path and the multipath, the faster the multipath power decaying and the smaller the ray arrival rate, the more improvement can be obtained by employment of switched beamforming arrays.

### Introduction

The wireless local area network (WLAN) uses orthogonal frequency division multiplexing (OFDM) technique to mitigate intersymbol interference (ISI). It is known that the smaller the channel delay spread, the smoother the frequency response and the smaller probability that the subcarrier will encounter deep fading. Using a directive antenna not only can increase the antenna gain, but also can suppress multipaths coming from the sidelobe directions. Hence, the channel delay spread can be reduced. However, if the transmitter and receiver positions are not known to each other, the mainbeam direction should be able to adaptively adjust. Using the switched beamforming arrays is the simplest way to achieve this purpose [1].

The Saleh-Valenzuela (S-V) model only considers the amplitude and time delay of each path component [2]. In this paper we will add the information of an angle of arrival (AOA) and an angle of departure (AOD) to each path component and use this model to study the switched beamforming arrays on WLAN transmission performance for different channel situations.

### Wideband Vector Indoor Channel Model

The S-V model assumes that rays arrive in clusters. The arrival times of the clusters and the rays in each cluster are modeled as Poisson arrival process. In the modified single cluster S-V model, the channel impulse response (CIR) is expressed by

$$h(t) = \sum_{l=0} \beta_l e^{j\theta_l} \delta(t - \tau_l) = \beta_0 \delta(t) + \sum_{l=1} \beta_l e^{j\theta_l} \delta(t - \tau_l)$$

where  $\beta_l$ ,  $\theta_l$  and  $\tau_l$  are the amplitude, phase and time delay of the  $l^{\text{th}}$  path component respectively.  $\theta_l$  is an independent random variable uniformly distributed over  $[0, 2\pi)$ .  $\tau_l$  can be described by a Poisson distribution with a mean arrival rate  $\lambda$ .  $\beta_0$  is the amplitude of the first path, and  $\beta_l$  is a random variable having the relationship  $\overline{\beta_l^2} = \exp(-\tau_l / \gamma)$  where  $\gamma$  is the power decay constant.

The S-V model implicitly assumes that the transmitter antenna and the receiver antenna are both omni-directional so that angular information of each multipath component can be ignored. When the antennas are directive, we have to further consider the angular information of the AOD and the AOA. To simplify the following discussion, we only consider the azimuthal pattern and neglect the elevation pattern. In indoor

environments, multipaths are resulted from reflections, diffractions and scattering. Since the transmitter and receiver can be placed at any position, it is reasonable to assume that the AOA and the AOD of each path are uniformly distributed over  $[0, 2\pi)$ .

When closely-spaced multiple antenna elements are employed in the transmitter side and/or the receiver side, we make two assumptions. First, the CIR of each transmitting and receiving element pair has the same multipath components, i.e., the same amplitude, time delay, AOA and AOD. Second, the wave of each multipath component is a plane wave. Under the above assumptions we can simulate the channel characteristics obtained by using multiple antenna elements.

### Performance of Switched Beamforming Array for Indoor WLAN

Now we compare the channel characteristics and transmission performance when switched beamforming arrays and omni-directional antennas are employed in WLAN system which utilizes the OFDM technology. The parameters of the WLAN system are according to IEEE 802.11a.

In this section both the transmitting array and receiving array have four elements which uniformly spaced with a spacing of half a wavelength. The weight of the  $m^{\text{th}}$  antenna element at either side can be expressed by  $W_m = \exp(j(m-1)\alpha)$  where  $\alpha$  can be  $45^\circ, 135^\circ, -135^\circ$  or  $-45^\circ$  depending on the desired beam direction [3]. The four beams of the switched beam array are shown in Fig. 1. Since the transmitting and receiving arrays both have 4 different beams, there are totally 16 beam combinations. We choose the beam combination with the largest output power as the desired beam combination.

Given a set of  $\{\beta_0, \gamma, \lambda\}$ , we randomly generate a large number of CIRs, and each multipath component is randomly assigned an AOA and an AOD. For each CIR, the corresponding receiving output of the switched beamforming array is calculated. The cumulative distribution functions (CDF) of the subcarrier power over the 20MHz bandwidth are shown in Fig. 2~4 for different sets of parameters.

The parameters shown in Fig. 2 are  $\gamma = 21.5\text{nsec}$ ,  $\lambda = 0.4\text{nsec}^{-1}$  and different values of  $\beta_0$ , 15dB, 5dB and -5dB. It is noted that  $\beta_0 = 15\text{dB}$  corresponds to the case of a strong LOS while  $\beta_0 = -5\text{dB}$  corresponds to the case of a high obstruction loss. We can see that the greater the  $\beta_0$ , the more improvement of power distribution by using switched beamforming arrays. Not only the CDF curve shifts to right, but also its slope is getting larger. Even though the LOS has been seriously obstructed, the switched beamforming array still has beamforming gain.

The parameters shown in Fig. 3 are  $\beta_0 = 10\text{dB}$ ,  $\lambda = 0.4\text{nsec}^{-1}$  and different values of  $\gamma$ , 17.2nsec, 28.6nsec and 43nsec. This is a case of having LOS since  $\beta_0 = 10\text{dB}$ . It is seen that the greater the attenuation constant, the greater the power distribution for the omni directional antenna. The beamforming gain is greater as  $\gamma$  is smaller.

The parameters shown in Fig. 4 are  $\beta_0 = 10\text{dB}$ ,  $\gamma = 21.5\text{nsec}$  and different values of  $\lambda$ ,  $0.2\text{nsec}^{-1}$ ,  $0.4\text{nsec}^{-1}$  and  $1\text{nsec}^{-1}$ . It is seen that for omni directional antennas, the power distribution is greater when the mean arrival rate is higher. However, after switched beamforming, they have comparable power distribution, which implies that channels with smaller mean arrival rate can have more beamforming gain.

Next we employ the channel responses to simulate the WLAN transmission performance. We plot the BER curves versus the mean signal to noise ratio (SNR), which is obtained by averaging all subcarrier powers over the 20MHz bandwidth for the SISO

(single input single output) case. Shown in Fig. 5~7 are plots of the BER curves for the SISO case and after switched beamforming. The channel parameter sets are the same as those used in the previous examples. The BER curve for the AWGN channel is also plotted for comparison. It is seen that after switched beamforming, the BER curves all shift to the left. If we define the minimum required SNR,  $(S/N)_{\min}$ , as the SNR gives a specific BER (for example,  $10^{-4}$ ), then we can obtain  $(S/N)_{\min}$  for each different parameter sets. It is seen that the required  $(S/N)_{\min}$  have been reduced after switched beamforming. However, the degree of improvement also depends on channel parameters. From these plots, we can conclude that the larger the  $\beta_0$ , the greater the attenuation slope of multipath components and the smaller the mean arrival rate, the more improvement can be obtained. This conclusion can be explained by the previous CDF plots of the subcarrier power of Fig. 2~4. Beamforming techniques can increase power gain and reduce delay spread. A smaller delay spread will result in a smoother subcarrier frequency response over the 20MHz bandwidth and therefore the probability that subcarrier power suffering deep fading will be much smaller.

### Conclusion

In this paper the vector wideband indoor channel model which includes not only the parameters of the S-V model but also the AOA and AOD of each path component has been presented. We use this channel model to study the channel characteristics and transmission performance obtained by using switched beamforming arrays at both the transmitter and the receiver. We found that a switched beamforming array can effectively increase the power gain, decrease the probability that the subcarrier encounters deep fading and reduce the required  $(S/N)_{\min}$  even when the LOS is seriously obstructed. However the degree of the improvement depends on the values of channel parameters. We found that the greater the  $\beta_0$ , the greater the attenuation slope of the multipath component and the smaller the mean arrival rate, the more improvement in transmission performance can be obtained by employment of switched beamforming arrays.

### Reference

- [1] J.C. Liberti and T.S. Rappaport, "Smart Antennas for Wireless Communications," Prentice-Hall PTR, 1999.
- [2] A. Saleh, R. Valenzuela, "A Statistical Model for Indoor Multipath Propagation," *IEEE Journal on Selected Area in Communications*, Vol. 5, No. 2, Feb 1987, pp. 128-137.
- [3] Robert S. Elliott, "Antenna Theory and Design," Prentice-Hall, Inc, 1981.

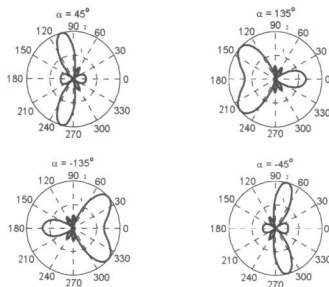


Fig. 1 Illustration of the switched beamforming array

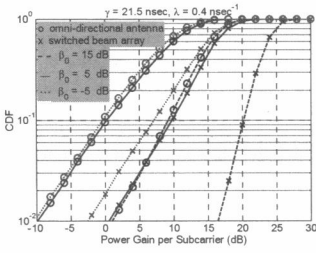


Fig. 2 CDF of the subcarrier power for the different values of  $\beta_0$

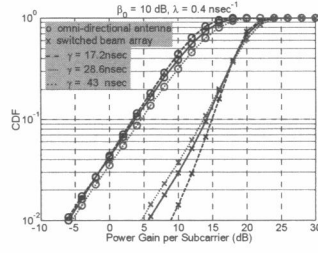


Fig. 3 CDF of the subcarrier power for the different values of  $\gamma$

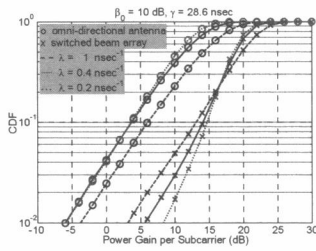


Fig. 4 CDF of the subcarrier power for the different values of  $\lambda$

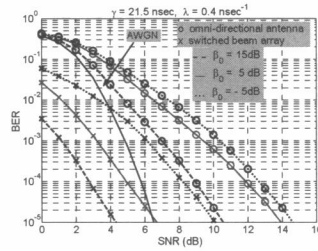


Fig. 5 Plots of the BER curves for the different values of  $\beta_0$

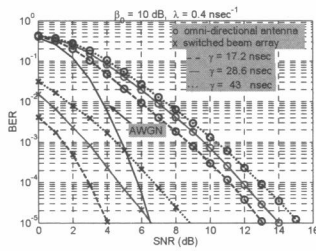


Fig. 6 Plots of the BER curves for the different values of  $\gamma$

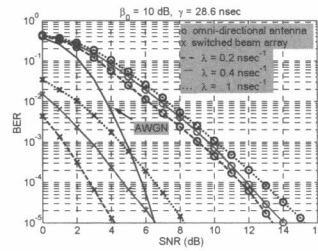


Fig. 7 Plots of the BER curves for the different values of  $\lambda$